Progress In Electromagnetics Research, Vol. 111, 419–432, 2011

EVANESCENT-MODE SUBSTRATE INTEGRATED WAVEGUIDE (SIW) FILTERS IMPLEMENTED WITH COMPLEMENTARY SPLIT RING RESONATORS

Q.-L. Zhang, W.-Y. Yin, and S. He

Centre for Optical and Electromagnetic Research
State Key Laboratory of MOI
Zhejiang University
Hangzhou 310058, China

L.-S. Wu

Key Laboratory of Ministry of Education for Research of Design and EMC of High-Speed Electronic Systems
Shanghai Jiao Tong University
Shanghai 200240, China

Abstract—A new type of evanescent-mode substrate integrated waveguide (SIW) bandpass filter is presented in this paper, with complementary split ring resonators (CSRRs) introduced on the top or bottom metal planes of the waveguide. Both positive and negative couplings are obtained between the CSRRs by changing their locations and orientations. In comparison with conventional SIW filters, the proposed filters are compact since their passbands are below the cutoff frequency of SIW. A third- and a fourth-order cross-coupled filter prototypes were designed using standard PCB technology. They operate at the same central frequency of 3.8 GHz, with their fractional bandwidths of 15% and 20%. The proposed filters have a wide upper stopband as the cutoff frequency of TE_{10}-mode in the SIW is much higher than the central frequency. Their good performance is demonstrated by both the simulated and measured S-parameters.

Received 3 November 2010, Accepted 6 December 2010, Scheduled 19 December 2010
Corresponding author: Qiao-Li Zhang (zhangqiaoli@coer.zju.edu.cn).

1. INTRODUCTION

Recently, substrate integrated waveguides (SIWs) have drawn much attention in the design of RF circuits, due to their advantages of high Q-factor, high power handling capability, low loss, and low cost [1]. The conventional SIW is synthesized by introducing two rows of metalized holes into the substrate, which can be fabricated using standard printed circuit board (PCB) and low-temperature co-fired ceramic (LTCC) technologies. Besides, SIWs are also easy to integrate with other planar circuits. Thanks to all of these benefits, there are a great number of applications in various circuit designs based on SIW technology [2–11].

However, when compared to microstrip, coplanar waveguide and slotline structures, the conventional SIWs are still large. In order to miniaturize the SIW while keeping its advantages, many methods have been proposed recently, such as ridging [12], folding [13], half-mode [14] and dielectric-loading [15], etc.. The evanescent-mode technique is also a good choice [16, 17]. By loading some specific elements, a SIW operating below its cutoff frequency can be achieved. Further, the evanescent-mode SIW components have attractive spurious suppression characteristics.

On the other hand, it is noted that the complementary split ring resonator (CSRR) has been used in the design of some slow-wave transmission lines, couplers and filters with high performance and compact size [18–22]. In particular, by combining highpass SIW with bandstop periodical CSSRs, SIW bandpass filters with wide passbands can be obtained [23, 24]. A CSRR is also utilized as a resonator in a dual-mode SIW cavity in order to build up an extended doublet SIW filter [25]. With the CSRRs introduced on the top metal plane, a novel compact SIW bandpass filter is presented in [26], with its passband located below the cutoff frequency of the dominant mode in SIW. Further, it is expected that the filter size can be reduced significantly by introducing some CSRRs both on its top and bottom metal planes, with its frequency selectivity and stopband rejection also improved.

In this paper, we present one type of new evanescent-mode SIW filter combined with specific CSRRs located both on the top and bottom metal planes, which can operate below the cutoff frequency of waveguide. In our design, both positive and negative couplings are obtained by controlling the locations and orientations of CSRRs. To validate our method, a third- and a fourth-order cross-coupled filter prototypes are realized, and good agreement between their simulated and measured results has been achieved. In comparison with the previous counterparts, our proposed SIW filters with CSRRs are

compact and have wide upper stopbands.

2. ANALYSIS AND DESIGN

2.1. Evanescent-mode SIW Loaded with CSRR

Figure 1 shows the configuration of SIW with etched CSRRs both on its top and bottom metal planes. For the design facility and the adjustment of coupling coefficient between adjacent resonators, the single split ring instead of double ring is used in our design. The CSRRs on the SIW surface are excited by the evanescent wave in the cutoff waveguide, and they are regarded as half-wavelength slotline resonators. Here, they resonate at about 3.8 GHz. The initial cutoff frequency of the designed SIW with the width of 12 mm should be at 8 GHz, and the passband of SIW loaded with CSRRs is below its cutoff frequency. In other words, the structure works as an evanescent-mode SIW loaded with embedded CSRR elements.

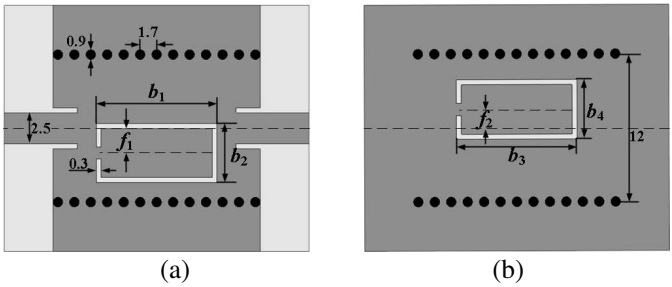

Figure 1. Layout of the evanescent-mode SIW etched with CSRRs both on its top and bottom metal planes: (a) its top view; and (b) bottom view.

Figure 2 shows the dispersion diagram of the evanescent-mode SIW loaded with CSRRs both on its top and bottom metal planes. When the offset distance $f_1 + f_2$ between the top and bottom CSRRs from their central lines is large enough, the coupling between them is relatively weak. There is only one passband found below the cutoff frequency of SIW in such a weak coupling case. However, in the case of a strong coupling, i.e., the lateral distance $f_1 + f_2$ between the CSRRs is small, two passbands appear below the cutoff frequency of SIW. Further, the first passband corresponding to strong coupling exhibits a positive slope and demonstrates one forward-wave feature, while backward-wave propagation is observed from the negative slope of the second passband of the strong coupling, which can be utilized to provide more freedoms for the design of some specific devices.

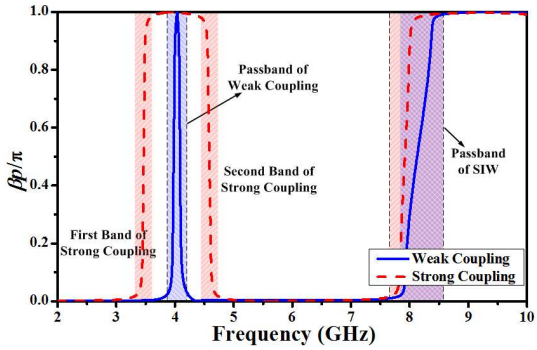

Figure 2. Dispersion diagram of the evanescent-mode SIW etched with CSRRs both on its top and bottom metal planes.

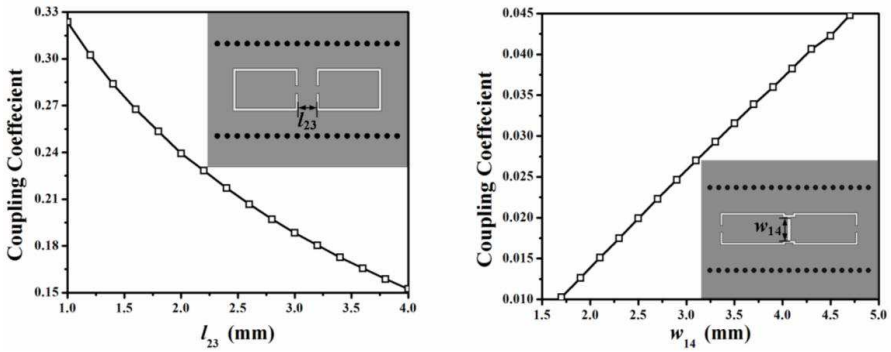

(a) (b)

Figure 3. Coupling structures and extracted coupling coefficients of the CSRRs etched on the same metal plane for (a) the face-to-face; and (b) back-to-back couplings.

2.2. Internal Couplings

To build up a filter based on the above configuration, the coupling between two adjacent CSRRs on the same metal plane can be implemented through the evanescent-mode SIW operating below the cut-off frequency of its dominant TE_{10}-mode. The section of evanescent-mode SIW can provide an inductive coupling [12], and the positive coupling coefficient between two face-to-face CSRRs is reduced rapidly when the length of the evanescent-mode SIW increases. Thus, a proper coupling coefficient can be obtained by adjusting its length between two CSRRs, as shown in Figure 3(a), where the coefficient is extracted by the commercial software, Ansoft HFSS.

Since the electric field in a CSRR reaches its maximum at its middle slot section, a capacitive coupling can be realized between two CSRRs etched on the same metal plane in the back-to-back configuration, as illustrated in Figure 3(b). To eliminate inductive influence of the evanescent-mode SIW, two coupled CSRRs directly share the same slot section. From Figure 3(b), it is seen that the longer the shared slot is, the stronger the coupling provided will be.

Unlike the previous case, the coupling between CSRRs located on different metal planes is always dominated by their electric fields. Figures 4(a) and (b) show the electric field distributions at the first eigen peak of the two coupled CSRRs, which are etched on different metal planes with the inverse side-to-side and side-to-face configurations, respectively. It can be seen that the electric fields of the two CSRRs have opposite directions in both cases. This indicates that the first eigenmode of them is a quasi-odd one, and the two CSRRs are electrically coupled with a negative coupling coefficient obtained.

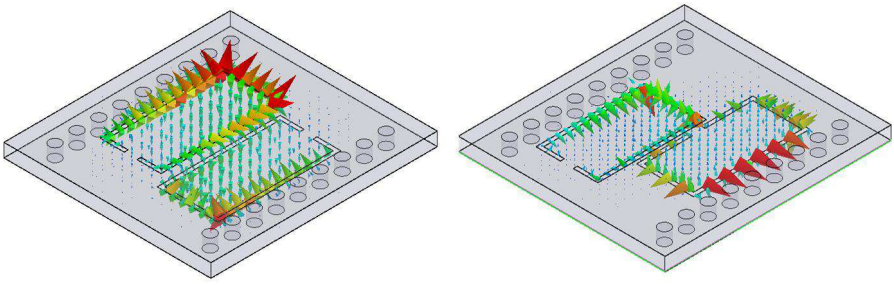

(a) (b)

Figure 4. Electric field distributions at the first eigen peak of two coupled CSRRs etched on different metal planes for (a) the inverse side-to-side; and (b) side-to-face couplings.

As shown in Figure 5, the parameters f_1 and f_2 are the offsets of CSRRs etched on the top and bottom metal planes from the central line of the evanescent-mode SIW, respectively. The dash lines represent the central lines of SIW and CSRRs. It is concluded that the coupling coefficient between two CSRRs located on the top and bottom metal planes of an evanescent-mode SIW can be controlled by adjusting the offset between them. The larger the offset is, the weaker the coupling will be.

Obviously, the scheme with CSRRs etched on both metal planes can provide more flexibility for the coupled resonators than the previous counterparts proposed in [17–20], which is useful for the design of evanescent-mode SIW filters with compact configurations.

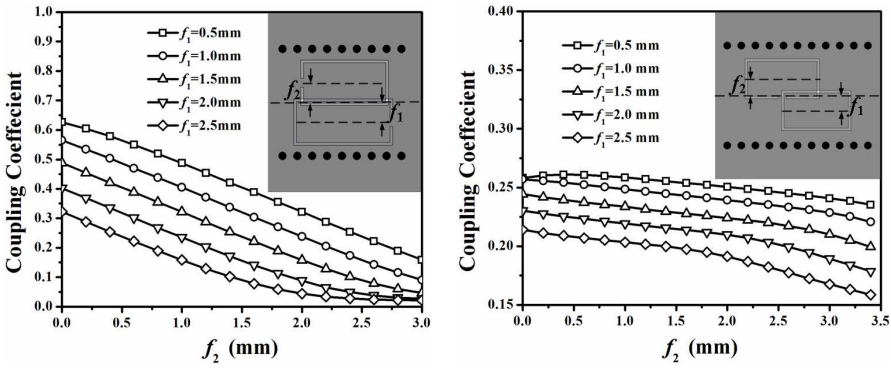

Figure 5. Coupling structures and their corresponding extracted coefficients of the CSRRs etched on different metal planes in (a) the inverse side-to-side; and (b) side-to-face couplings.

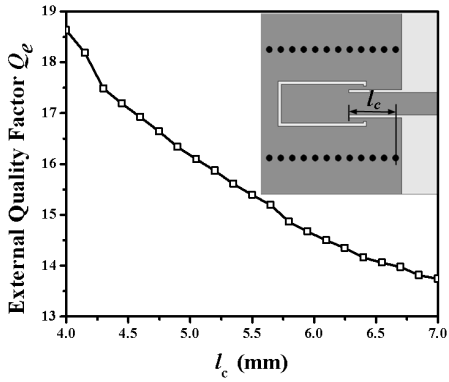

Figure 6. External Q-factor of the proposed excitation structure as a function of insertion length denoted by l_c.

2.3. External Coupling

In order to determine the external Q-factor of CSRR, numerical analysis is carried out using HFSS, where the CSRR is excited by a 50-Ω microstrip feed-line inserted into it so as to obtain a strong external coupling. Figure 6 shows that the external Q-factor can be accurately determined by the insertion length. Then, a properly selected excitation structure is determined to satisfy our design specifications.

2.4. Bandpass Filter Configurations

To demonstrate our design method, a third- and a fourth-order cross-coupled bandpass filters are realized, based on the evanescent-mode SIW embedded with CSRRs both on its top and bottom metal planes. Their coupling topologies are plotted in Figure 7. The coupling matrices of the third- and fourth-order prototypes are synthesized, with the same central frequency of $f_0 = 3.8\,\text{GHz}$ and their individual fractional bandwidths of FBW = 15% and 20%, respectively. The designed in-band return loss of the filters is $-20\,\text{dB}$, the transmission zeros are located at 3.2 GHz for the third-order filter, and 2.7 and 4.5 GHz for the fourth-order one.

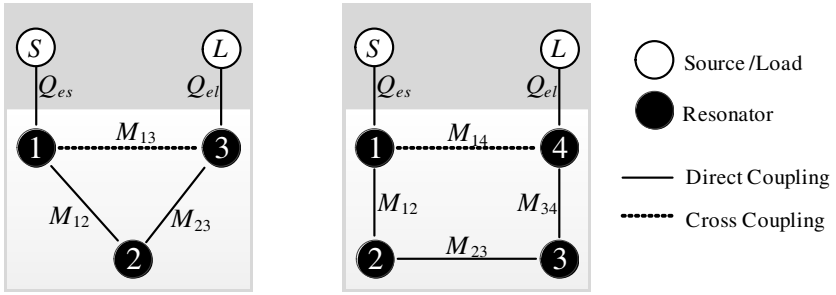

Figure 7. Coupling topologies of (a) the third- and (b) the fourth-order cross-coupled bandpass filters.

Figures 8 and 9 show the geometries of the third- and the fourth-order filters, respectively, with their geometrical parameters also given. For both cases, a pair of CSRRs, etched on the top metal plane of the evanescent-mode SIW, are cross-coupled with each other, and they are also excited by microstrip feedlines. In the third-order case, two negative couplings between the CSRRs located on different metal planes are included in the direct-coupling path. In the fourth-order case, an additional magnetic coupling between two CSRRs etched on the bottom metal plane of evanescent-mode SIW is utilized for direct coupling. They are all realized according to the above structures given in Figures 3–6. As shown in Figure 9(a), the stepped slots are also used in the excitation structure of the fourth-order filter so as to obtain better external coupling.

According to the design curves of the internal and external coupling coefficients given in Sections 2.2 and 2.3, all initial dimensions of both prototypes are determined by adjusting the lengths of the coupling side, the distance and offset between the embedded CSRRs,

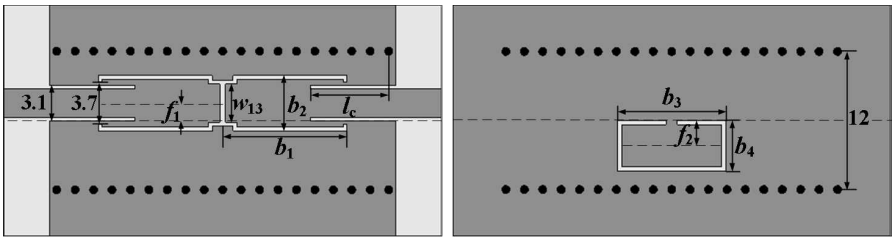

Figure 8. Geometry of the third-order filter prototype: (a) its top view; and (b) bottom view (unit: mm).

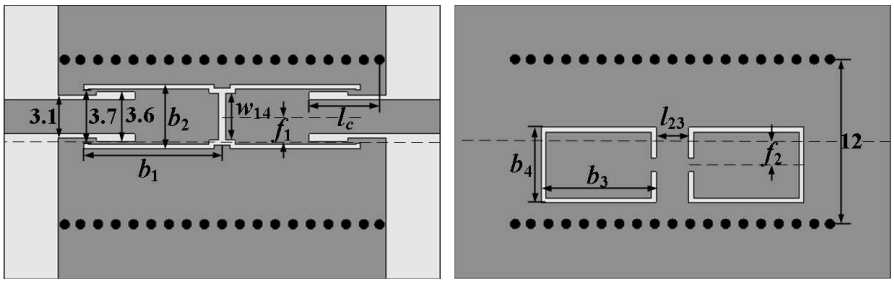

Figure 9. Geometry of the fourth-order filter prototype: (a) its top view; and (b) bottom view (unit: mm).

and the insertion length of feedlines. Further, certain optimization should be performed for the whole structure by taking all coupling effects into account.

3. RESULTS AND DISCUSSIONS

Figure 10 shows the photos of two filters. They were fabricated on the F4B-2 substrate, with the relative permittivity of $\varepsilon_r = 2.65$, the loss tangent of $\tan\delta = 0.003$, and the thickness of $h = 1.0\,\text{mm}$. All metallic via-holes of the SIW structures have a diameter of 0.9 mm, and the center-to-center spacing is set to 1.7 mm. The other geometrical parameters presented in Figures 8 and 9 are summarized in Table 1. The overall sizes of the third- and the fourth-order prototypes, excluding their excitation structures, are $21.6 \times 12\,\text{mm}^2$ $(0.45 \times 0.24\lambda_g^2)$ and $21.4 \times 12\,\text{mm}^2$ $(0.44 \times 0.24\lambda_g^2)$, respectively, where λ_g is the guided wavelength in the substrate at the central frequency. The third-order

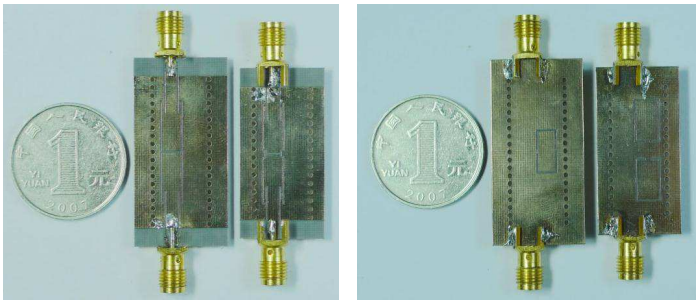

(a) (b)

Figure 10. Photos of the proposed bandpass filters: (a) their top view; and (b) bottom view.

Table 1. Critical dimensions of the two evanescent-mode SIW filters implemented with CSRRs (Unit: mm).

Symbol	Third-Order	Fourth-Order	Symbol	Third-Order	Fourth-Order
b_1	9.9	10.1	f_1	2	1.9
b_2	4.8	4.6	f_2	1.9	1.92
b_3	9.35	9.15	w_{13}	4.8	/
b_4	4.4	5.4	l_c	7.2	6.6
l_{23}	/	3.45	w_{14}	/	3.6

SIW filter, loaded with CSRRs only on its top metal plane in [26], occupies an area of $0.60 \times 0.30\lambda_g^2$. Thus, by loading etched patterns on both metal planes of the evanescent-mode SIW, a size reduction of about 40% is achieved in our developed third-order prototype.

The measured S-parameters of the third- and fourth-order components are plotted in Figures 11(a) and (b), respectively, which agree well with the simulated ones. There is a small discrepancy between the measured and simulated S-parameters, which is mainly caused by the fabrication tolerance. It has certain effects on the coupling coefficients between CSRRs on the top and bottom metal planes of evanescent-mode SIW.

The measured central frequencies of two filters are about 3.78 and 3.82 GHz, with 3-dB bandwidths of 600 and 780 MHz, respectively. For the third-order one, its in-band insertion loss is lower than 1.75 dB. An obvious spurious response arises around 11.0 GHz. From the electric field shown in Figure 12(a), it can be seen that the parasitic response is introduced by the TE_{10}-mode of the SIW. Then, the stopband attenuation of the third-order prototype is better than 15 dB from 4.6

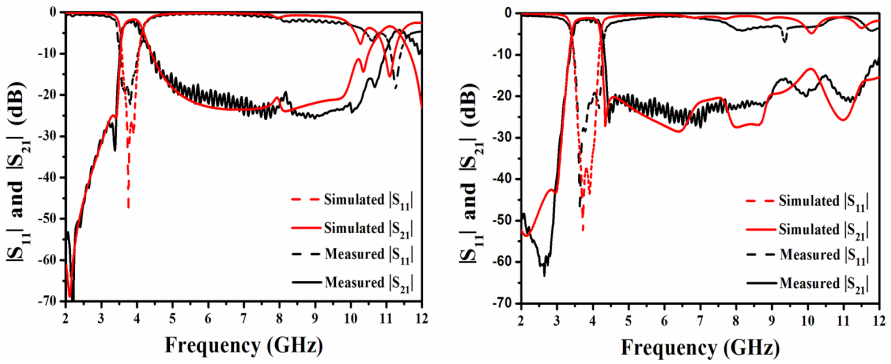

Figure 11. Simulated and measured S-parameters of the fabricated bandpass filters of (a) the third- and (b) the fourth-order prototypes.

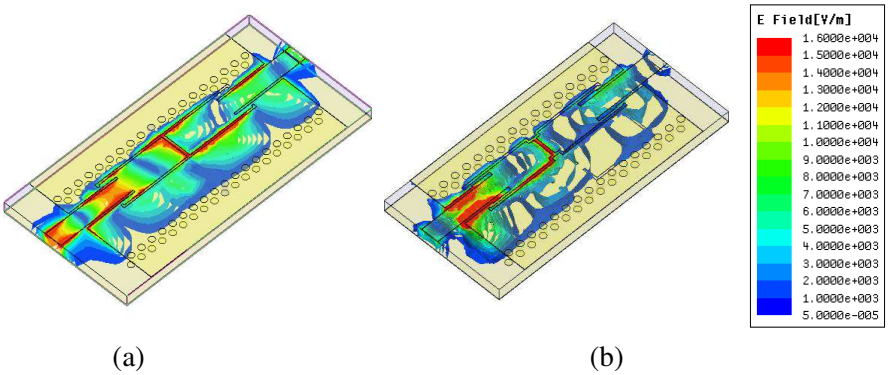

Figure 12. Electric field distributions of the parasitic responses of the proposed filters for: (a) the third-order filter at 11.0 GHz; and (b) the fourth-order filter at 9.0 GHz.

to 10.8 GHz. For the fourth-order one, the measured insertion loss is about 1.0 dB and the out-of-band rejection level exceeds 20 dB within a frequency range lower than 9.0 GHz. This is due to that the TE_{10}-mode propagation in the SIW is suppressed by the slots of the etched CSRRs, as shown in Figure 12(b). The group delays of S_{21} over the most frequency range of the passband are plotted in Figure 13. As shown, the measured group delays of the proposed filters agree well with the simulated ones. Since they are not designed for flat group delay, the variation in group delays is a little large.

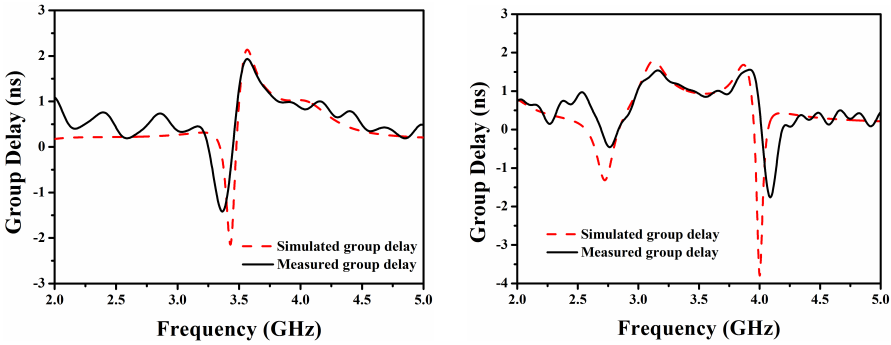

Figure 13. The simulated and measured group delay of (a) the third- and (b) the fourth-order filters as functions of frequency.

4. CONCLUSION

A new type of evanescent-mode SIW filter embedded with CSRRs both on the top and bottom metal planes of the waveguide is presented in this paper, where the passband is located below the cutoff frequency of the dominant mode in SIW. By choosing the locations and orientations of CSRRs appropriately, both inductive and capacitive internal couplings can be realized between the patterns etched on the same or different metal planes. The proposed cross-coupled bandpass filter is compact, when compared with the previous SIW counterparts. The new SIW filters also have good spurious suppression characteristics. Two cross-coupled filter prototypes were designed and fabricated so as to validate our design method, with good agreement obtained between their simulated and measured S-parameters.

ACKNOWLEDGMENT

Wen-Yan Yin and Lin-Sheng Wu appreciated the financial support by the National Basic Research Program under Grant 2009CB320204 and the National Science Foundation under Grant 60831002 of China.

REFERENCES

1. Piloto, A., K. Leahy, B. Flanick, and K. A. Zaki, "Waveguide filters having a layered dielectric structures," U.S. Patent 5382931, Jan. 1995.

2. Chen, X., K. Wu, and Z. Li, "Dual-band and triple-band substrate integrated waveguide filters with Chebyshev and quasi-elliptic responses," *IEEE Trans. Microw. Theory Tech.*, Vol. 55, No. 12, 2569–2578, Dec. 2007.
3. Zhou, Y. and S. Lucyszyn, "Modelling of reconfigurable terahertz integrated architecture (Retina) SIW structures," *Progress In Electromagnetics Research*, Vol. 105, 71–92, 2010.
4. Hu, G., C. Liu, L. Yan, K. Huang, and W. Menzel, "Novel dual mode substrate integrated waveguide band-pass filters," *Journal of Electromagnetic Waves and Applications*, Vol. 24, No. 11–12, 1661–1672, 2010.
5. Wang, Z., X. Zeng, B. Yan, R. M. Xu, and W. Lin, "A millimeter-wave *E*-plane band-pass filter using multilayer low temperature co-fired ceramic (LTCC) technology," *Journal of Electromagnetic Waves and Applications*, Vol. 24, No. 1, 71–79, 2010.
6. Souzangar, P. and M. Shahabadi, "Numerical multimode thru-line (TL) calibration technique for substrate integrated waveguide circuits," *Journal of Electromagnetic Waves and Applications*, Vol. 23, No. 13, 1785–1793, 2009.
7. Song, Q. Y., H. R. Cheng, X. H. Wang, L. Xu, X. Q. Chen, and X. W. Shi, "Novel wideband bandpass filter integrating HMSIW with DGS," *Journal of Electromagnetic Waves and Applications*, Vol. 23, No. 14–15, 2031-2040, 2009.
8. Lin, S., S. Yang, A. E. Fathy, and A. Elsherbini, "Development of a novel UWB vivaldi antenna array using SIW technology," *Progress In Electromagnetics Research*, Vol. 90, 369–384, 2009.
9. Hammou, D., E. Moldovan, and S. O. Tatu, "V-band microstrip to standard rectangular waveguide transition using a substrate integrated waveguide (SIW)," *Journal of Electromagnetic Waves and Applications*, Vol. 23, No. 2–3, 221–230, 2009.
10. Tao, Y. and Z. X. Shen, "Broadband substrate integrated waveguide orthomode transducers," *Journal of Electromagnetic Waves and Applications*, Vol. 23, No. 16, 2099–2108, 2009.
11. Li, R.-Q., X.-H. Tang, and F. Xiao, "A novel substrate integrated waveguide square cavity dual-mode filter," *Journal of Electromagnetic Waves and Applications*, Vol. 23, No. 17–18, 2523–2529, 2009.
12. Rong, Y., K. A. Zaki, M. Hageman, D. Stevens, and J. Gipprich, "Low-temperature cofired ceramic (LTCC) ridge waveguide bandpass chip filters," *IEEE Trans. Microw. Theory Tech.*, Vol. 47, No. 12, 2317–2324, Dec. 1999.

13. Grigoropoulos, N., B. Sanz-Izquierdo, and P. R. Young, "Substrate integrated folded waveguides (SIFW) and filters," *IEEE Microw. Wireless. Compon. Lett.*, Vol. 15, No. 12, 829–831, Dec. 2005.
14. Wang, Y. Q., W. Hong, Y. D. Dong, B. Liu, H. J. Tang, J. X. Chen, X. X. Yin, and K. Wu, "Half mode substrate integrated waveguide (HMSIW) bandpass filter," *IEEE Microw. Wireless. Compon. Lett.*, Vol. 17, No. 4, 265–267, Apr. 2007.
15. Wu, L., L. Zhou, X. Zhou, and W. Yin, "Bandpass filter using substrate integrated waveguide cavity loaded with dielectric rod," *IEEE Microw. Wireless. Compon. Lett.*, Vol. 19, No. 8, 491–493, Aug. 2009.
16. Ruiz-Cruz, J. A., Y. C. Zhang, M. M. Fahmi, and K. A. Zaki, "Ridge waveguide elliptic filters in narrow-wall canonical configuration," *Proc. 36th Eur. Microwave Conf.*, 1080–1082, Manchester, UK, Sep. 2006.
17. Wu, L., X. Zhou, W. Yin, L. Zhou, and J. Mao, "A substrate integrated evanescent-mode waveguide filter with nonresonating node in low-temperature co-fired ceramic," *IEEE Trans. Microw. Theory Tech.*, Vol. 58, No. 10, 2654–2662, Oct. 2010.
18. Falcone, F., T. Lopetegi, J. D. Baena, R. Marques, F. Martin, and M. Sorolla, "Effective negative-epsilon stopband microstrip lines based on complementary split ring resonators," *IEEE Microw. Wireless. Compon. Lett.*, Vol. 14, No. 6, 280–282, Jun. 2004.
19. Mondal, P., M. K. Mandal, A. Chaktabarty, and S. Sanyal, "Compact bandpass filters with wide controllable fractional bandwidth," *IEEE Microw. Wireless. Compon. Lett.*, Vol. 16, No. 10, 540–542, Oct. 2006.
20. Gil, M., J. Bonache, J. G. García, J. Martel, and F. Martín, "Composite right left-handed metamaterial transmission lines based on complementary split rings resonators and their applications to very wideband and compact filter design," *IEEE Trans. Microw. Theory Tech.*, Vol. 55, No. 6, 1296–1304, Jun. 2007.
21. Deng, J. Y., Y. Z. Yin, X. S. Ren, and Q. Z. Liu, "Study on a dual-band notched aperture UWB antenna using resonant strip and CSRR," *Journal of Electromagnetic Waves and Applications*, Vol. 23, No. 5–6, 627–634, 2009.
22. Li, X., L. Yang, S.-X. Gong, and Y.-J. Yang, "A novel tri-band-notched monopole antenna," *Journal of Electromagnetic Waves and Applications*, Vol. 23, No. 1, 139–147, 2009.
23. Zhang, X., Z. Yu, and J. Xu, "Novel band-pass substrate

integrated waveguide (SIW) filter based on complementary split ring resonators (CSRRs)," *Progress In Electromagnetics Research*, Vol. 72, 39–46, 2007.

24. Che, W., C. Li, K. Deng, and L. Yang, "A novel bandpass filter based on complementary split rings resonators and substrate integrated waveguide," *Microw. Opt. Technol. Lett.*, Vol. 50, No. 3, 699–701, Mar. 2008.
25. Wu, L., X. Zhou, Q. Wei, and W. Yin, "An extended doublet substrate integrated waveguide (SIW) bandpass filter with a complementary split ring resonator (CSRR)," *IEEE Microw. Wireless. Compon. Lett.*, Vol. 19, No. 12, 777–779, Dec. 2009.
26. Dong, Y., T. Yang, and T. Itoh, "Substrate integrated waveguide loaded by complementary split-ring resonators and its applications to miniaturized waveguide filters," *IEEE Trans. Microw. Theory Tech.*, Vol. 57, No. 9, 2211–2223, Sep. 2009.